ARTICLE

Production of a Fluorescence Resonance Energy Transfer (FRET) Biosensor Membrane for MicroRNA Detection

Received 00th January 20xx,
Accepted 00th January 20xx

DOI: 10.1039/x0xx00000x

www.rsc.org/

Yike Fu[a], Tong Chen[a], Tongxu Gu[a], Yuxi Xie[a], Yu Luo[a], Gang Wang[a], Congkun Xie[a], Jie Huang[b], Xiang Li[a]*, Serena Best[c], Gaorong Han[a]*

MicroRNAs (miRNAs) play a key role in regulating gene expression but can be associated with abnormalities linked to carcinogenesis and tumor progression. Hence there is increasing interest in developing methods to detect these non-coding RNA molecules in the human circulation system. Here, a novel FRET miRNA-195 targeting biosensor, based on silica nanofibers incorporated with rare earth-doped calcium fluoride particles (CaF_2:Yb,Ho@SiO_2) and gold nanoparticles (AuNPs), is reported. The formation of a sandwich structure, as a result of co-hybridization of the target miRNA which is captured by oligonucleotides conjugated at the surface of CaF_2:Yb,Ho@SiO_2 fibers and AuNPs, brings the nanofibers and AuNPs into close proximity and triggers the FRET effect. The intensity ratio of green to red emission, I_{541}/I_{650}, was found to decrease linearly with increasing concentration of the target miRNA and this can be utilized as a standard curve for quantitative determination of miRNA concentration. This assay offers a simple and convenient method for miRNA quantification, with the potential for rapid and early clinical diagnosis of diseases such as breast cancer.

1 Introduction

There is increasing concern about the very high numbers of breast cancer-related deaths worldwide. In 2012, there were more than 1.7 million diagnosed cases, 521,900 deaths and overall, the disease represents 15% of cancer deaths in the female population.[1] Hence, there is an urgent need for the development of early detection methodologies to expand and inform treatment options and offer the potential for improved clinical outcome.

MicroRNAs (miRNAs), a class of small noncoding RNA molecules (~22 nucleotides in length), are thought to be involved in the regulation of ~30 % of human genes and to play a role in a range of biological processes including, the cell cycle, differentiation and metabolism. [2-5] They are also believed to be associated with human diseases such as diabetes, neurodegenerative or immuno- disorders and cancer.[5] The de-regulation or dysfunction of miRNAs plays an important role in carcinogenesis and disease progression. Since the existence of miRNAs in the circulatory system was confirmed, the expression profile of serum miRNAs has emerged as a promising and convenient diagnostic bio-marker for non-invasive, early-stage disease detection.[6, 7] MiRNA-195 (miR-195) has been shown to play an important role in breast tumorigenesis.[8] For example, blood-based miRNA profiling studies demonstrated that systemic miR-195 levels were raised in breast cancer patients, but decreased after surgery.[9, 10] Thus, rapid and efficient detection of miR-195 is essential for early diagnosis of breast cancer.

However, the detection of miRNAs in clinical samples is challenging due to their short sequences, single base differences and extremely low concentration.[11, 12] Various sensing mechanisms have been developed for miRNA measurement, including electrochemical and electromechanical biosensing and surface plasmon resonance.[13-15]

Fluorescence resonance energy transfer (FRET), in which the electronic excitation energy of an energy donor chromophore is transferred to an energy acceptor in the presence of a target, has been used previously in miRNA detection.[16-18] Traditional fluorophores used in FRET-based detection include Cy5, FAM and Texas red. However, these are limited by intrinsic drawbacks including broad emission bands and photobleaching effects.[19]

To address these issues, alternative methods have been explored, such as those based on upconversion photoluminescent (UCPL) nanomaterials. These materials offer the advantages of high quantum yields, narrow emission peaks, long lifetimes, superior photostability, deep penetration and low toxicity.[20-24] More importantly, upconversion is a process where low-energy light, (usually near-infrared (NIR) or infrared (IR)) is converted to higher-energy light (UV or visible), through multiple photon absorptions or energy transfers. This property does not occur in natural biological materials.[25, 26] Therefore, there is no background auto-fluorescence

[a] *State Key Laboratory of Silicon Materials, School of Materials Science and Engineering, Zhejiang University, Hangzhou, Zhejiang 310027, P. R. China.*
[b] *Department of Mechanical Engineering, University College London, London WC1E 7JE, UK.*
[c] *Department of Materials Science and Metallurgy, University of Cambridge, Cambridge CB3 0FS, UK.*
* *E-mail: xiang.li@zju.edu.cn; hgr@zju.edu.cn*

Electronic Supplementary Information (ESI) available: Diameter distribution of CaF_2:Yb,Ho nanoparticles hydrothermally at 180 °C for 24 h. SEM and TEM of CaF_2:Yb,Ho nanoparticles calcined at 700 °C for 4 h. Simplified energy level scheme of Yb^{3+}/Ho^{3+} ions with mechanisms of energy transfer under excitation of 980 nm NIR. UV-vis absorption of CaF_2:Yb,Ho@SiO_2-NH_2, Probe 1 and CaF_2:Yb,Ho@SiO_2-Probe 1 conjugation. See DOI: 10.1039/x0xx00000x

from biological systems, which means that the signal-to-noise ratio and sensitivity of the detection is high.[27] These advantages have made UCPL materials an ideal choice as the fluorescence donor in FRET-based biological detection.

Fluoride materials (such as $NaYF_4$) have been investigated extensively as matrices for rare earth doping[28-30] and, in particular, the unique NIR-to-visible UCPL properties and low phonon energies of CaF_2 nanomaterials offer the potential to minimize multiphonon de-excitation. In addition, when these materials are doped with rare earth elements, the energy transfer rate can be accelerated due to charge compensation effects, the promotion of pair formation and the influence on lattice structure - all of which enhance the probability of UC.[31, 32] However, despite these advantages, there appears to have been little work on the use of rare earth-doped CaF_2 in FRET-based technology for the detection of biomolecules such as miRNA. To date reports have focused on the production of CaF_2:Yb,Ho for optical applications[33] and the use of CaF_2:Ce,Tb in avidin and uPAR detection in particulate form[34].

Gold nanoparticles (AuNPs) have been used extensively to quench fluorescence signals. They have also been used in gene delivery applications[35-37], and have been used to detect immunoglobulin G and ss-DNA[38, 39], but there does not appear to have been work reported on the detection of miRNA-195 sequences.

In a FRET-based detection system, it is necessary to ensure a spectral overlap between the emission of the donor and the absorption of acceptor. The absorption of gold nanoparticles with a diameter of 10-20 nm is usually located in the green region.[19, 40] Therefore, strong green emission from the energy donor is essential for FRET effects, in order to optimise the sensitivity.

Photoluminescent CaF_2:Yb,Er embedded in SiO_2 nanofibers have been used in drug delivery[41]. However, the fact that silica nanofibers have a high surface area and also offer a high density of OH groups on their surface means that they have the capacity to bind high numbers of DNA probes along their fiber surfaces and thereby offer the potential to facilitate miRNA detection. The processing properties of the nanofibers means that they can be processed to form a membrane and hence offer high levels of ease of handling.

Therefore, in order to develop a practical and functional biosensor, in this study, Yb and Ho co-doped CaF_2 (CaF_2:Yb,Ho) nanoparticles were synthesized using a hydrothermal process and were incorporated into electrospun SiO_2 nanofibers (CaF_2:Yb,Ho@SiO_2) (Figure 1).

Two complementary miRNA-capturing oligonucleotides were selected to bind to two either end of the same miRNA target molecule. The CaF_2:Yb,Ho@SiO_2 nanofibers were modified with amino groups to interact with a carboxyl group-functionalized miRNA-capturing oligonucleotide (Probe 1). Gold nanoparticles were conjugated with a thiol-modified miRNA-capturing oligonucleotide (Probe 2). When miRNA-195 was added into the system, it was therefore captured by the two different oligonucleotides and a sandwich-like complex was formed, as shown in Figure 1. Via this sandwich-type hybridization, the process led to AuNPs and CaF_2:Yb,Ho@SiO_2 nanofibers being brought sufficiently close together to trigger the FRET effect, and the green emission of CaF_2:Yb,Ho@SiO_2 nanofibers was absorbed by the AuNPs. By measuring the change in the fluorescence properties under 980 nm irradiation, a quantitative measurement of the target miRNA can be obtained.

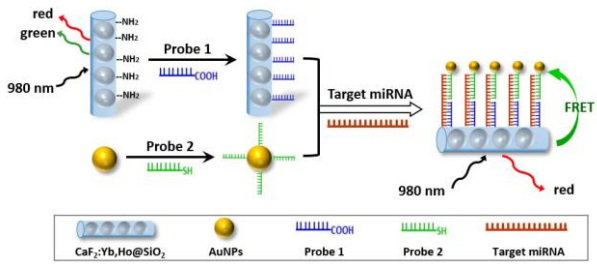

Figure 1 Schematic illustration for the synthesis of miRNA nanosensor based on CaF_2:Yb,Ho@SiO_2 nanofibers and AuNPs.

Table 1 Sequences of the oligonucleotides.

Primer Name	Sequence (5′ to 3′)
miRNA-capturing oligonucleotide 1 (Probe 1)	5′-COOH AAAAGCCAATATTTC-3′
miRNA-capturing oligonucleotide 2 (Probe 2)	5′-TGTGCTGCTAAAAAA SH-3′
miR-195 (target miRNA)	5′-UAGCAGCACAGAAAUAUUGGC-3′

2 Results and discussion

2.1 CaF_2:Yb,Ho nanoparticles

Scanning electron microscopy (SEM) indicated that the CaF_2:Yb,Ho nanoparticles synthesized hydrothermally at 180 °C were spheroidal in morphology with a relatively monodisperse particle size of approximately 320 nm (Figure 2a). Figure S1 shows the particle diameter distribution. Transmission electron microscopy (TEM) revealed that the spheroidal nanoparticles were composed of aggregates of primary crystallites (Figure 2b). Lattice imaging using HRTEM shows clear lattice fringes indicating that the nanoparticles were highly crystalline (Figure 2c). Interplanar spacings of 0.276 nm and 0.310 nm were measured in two adjacent crystals and these dimensions correspond to the (200) and (111) planes of CaF_2 respectively (JCPDS No. 35-0816). The XRD pattern for the CaF_2:Yb,Ho nanoparticles shows that all of the diffraction peaks matched well with the standard pattern for cubic CaF_2 (JCPDS No. 35-0816) (Figure 3d). No obvious impurity peaks were observed, suggesting that the Yb^{3+} and Ho^{3+} ions were successfully incorporated into CaF_2 lattice. After sintering at

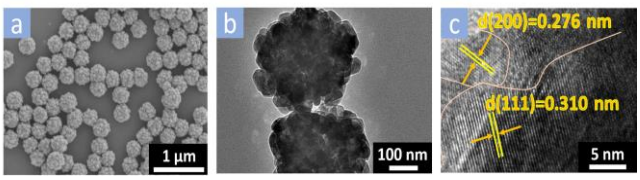

Figure 2 (a) SEM (b) TEM and (c) HRTEM images of CaF_2:Yb,Ho nanoparticles produced using hydrothermal synthesis at 180 °C.

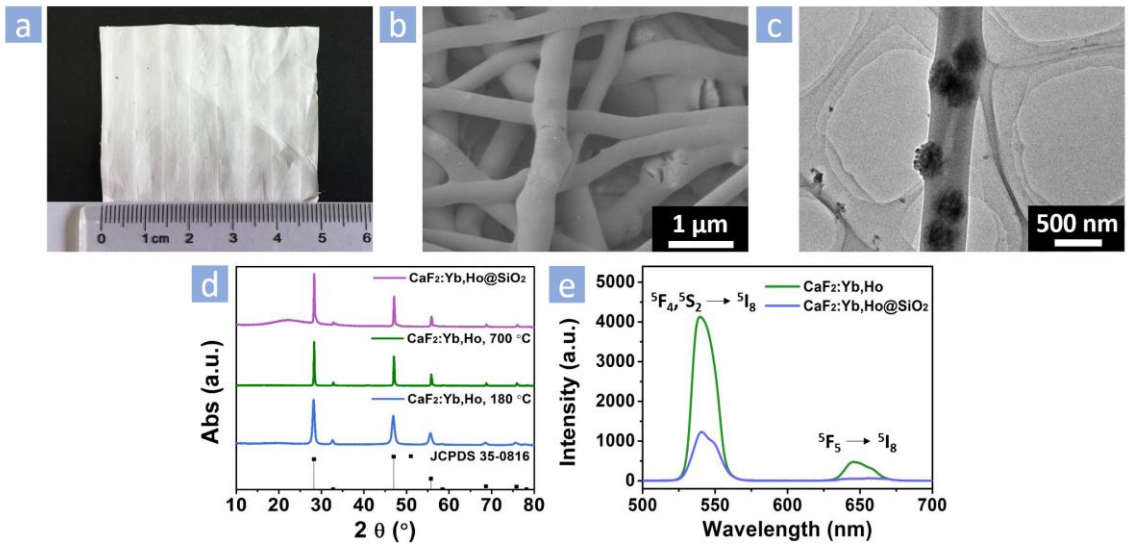

Figure 3 (a) Optical image of CaF_2:Yb,Ho@SiO_2 nanofiber membrane. (b) SEM (c) TEM images of CaF_2:Yb,Ho@SiO_2 nanofibers. (d) XRD patterns of CaF_2:Yb,Ho nanoparticles hydrothermally at 180 °C for 24 h (blue), CaF_2:Yb,Ho nanoparticles calcined at 700 °C for 4 h (green), CaF_2:Yb,Ho@SiO_2 nanofibers (purple) and the standard profiles of CaF_2 (JCPDS 35-0816) (black). (e) Upconversion photoluminescence spectra of CaF_2:Yb,Ho nanoparticles calcined at 700 °C for 4 h and CaF_2:Yb,Ho@SiO_2 nanofibers.

700 °C, the nanoparticles had a similar morphology to the uncalcined material (Figure S2), but the sharper XRD peaks suggested that crystallinity had increased. Under irradiation at 980 nm, the CaF_2:Yb,Ho nanoparticles exhibited two main upconversion emissions (Figure 3e). The green emission at about 541 nm is ascribed to the $^5F_4,^5S_2 \rightarrow ^5I_8$ transition, and the relatively weak red emission at about 650 nm is assigned to a $^5F_5 \rightarrow ^5I_8$ transition (Figure S3).[42] Yb^{3+} ions act as sensitizers in the system, which absorb infrared radiation (980 nm) and non-radiatively transfer their excitation to Ho^{3+} ions, thus populating not only the emitting levels but also the intermediate levels.[43, 44]

2.2 Electrospinning of CaF_2:Yb,Ho@SiO_2 nanofibers

The CaF_2:Yb,Ho@SiO_2 nanofibers were prepared by electrospinning. Figure 3a shows an optical image of an electrospun CaF_2:Yb,Ho@SiO_2 nanofiber membrane. Using SEM, the composite nanofibers were observed to have a smooth surface morphology and a diameter of approximately 490 nm (Figure 3b). TEM images revealed that the CaF_2:Yb,Ho nanoparticles were uniformly-distributed and along the length of the SiO_2 nanofibers (Figure 3c). The presence of amorphous SiO_2 was also confirmed from the XRD trace (Figure 3d), by the presence of a broad peak at ~23 °. The other sharp peaks, which are similar to the pattern of CaF_2:Yb,Ho nanoparticles, can be assigned to the particle phase in the nanofibers. In addition, the upconversion photoluminescence spectrum of CaF_2:Yb,Ho@SiO_2 nanofibers under 980 nm irradiation was similar to the spectrum of the CaF_2:Yb,Ho nanoparticles, although emission intensity was weakened by 75 % when the particles were incorporated into SiO_2. This was due to the quenching effect of surface groups with high vibration frequency, such as -OH groups on the SiO_2 nanofibers. Sol–gel SiO_2 nanofibers have been investigated widely in nanomedicine due to their biocompatibility and ease of chemical decoration. The CaF_2:Yb,Ho particle embedded SiO_2 nanofibers produced in this work, possess the advantages of SiO_2 nanofibers while ensuring the upconversion photoluminescence features of CaF_2:Yb,Ho nanoparticles allowing the detection of miRNA *via* a FRET effect.

2.3 Conjugation of Probe 1 with CaF_2:Yb,Ho@SiO_2

Prior to oligonucleotide conjugation, the CaF_2:Yb,Ho@SiO_2 nanofibers were functionalized with amino groups using APTES. The CaF_2:Yb,Ho@SiO_2 nanofibers were characterized before- and after amino modification using FTIR to demonstrate surface functionalization (Figure 4a). The FTIR spectrum of the CaF_2:Yb,Ho@SiO_2 nanofibers reveals a typical Si-O-Si asymmetric stretching vibration at 1093 cm^{-1}, Si-O-Si symmetric stretching vibration at 808 cm^{-1}, and Si-O-Si bending vibration at 464 cm^{-1}, which can be attributed to the SiO_2 matrix. After amino functionalization, a new peak at 1560 cm^{-1} appeared, which can be assigned to N-H stretching. The functionalization was also verified by studying changes in the zeta potential at various stages in the production process. For unfunctionalized CaF_2:Yb,Ho@SiO_2 nanofibers, the zeta potential is -13 mV due to the abundance of Si-OH groups on

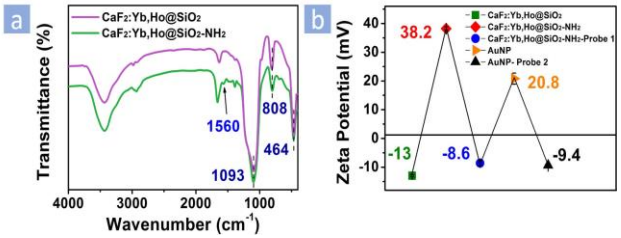

Figure 4 (a) FTIR spectra CaF_2:Yb,Ho@SiO_2 nanofibers before and after amino modification. (b) Zeta potentials of CaF_2:Yb,Ho@SiO_2 nanofibers, CaF_2:Yb,Ho@SiO_2 -NH_2 nanofibers, CaF_2:Yb,Ho@SiO_2-Probe 1, AuNPs, and Probe 2-conjugated AuNPs.

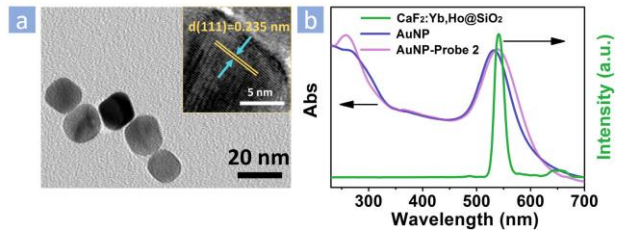

Figure 5 (a) SEM and (inset) TEM images of AuNPs; (b) UV-vis absorption of AuNPs and AuNP- Probe 2, and UCPL spectra of CaF_2:Yb,Ho@SiO_2 nanofibers.

the surface (Figure 4b). After amino functionalization, the surface charge was reversed to + 38.2 mV. These data indicate the successful amino modification of the CaF_2:Yb,Ho@SiO_2 nanofibers to form CaF_2:Yb,Ho@SiO_2-NH_2.

Subsequently, a carboxyl group-modified probe (Probe 1) was covalently grafted onto the CaF_2:Yb,Ho@SiO_2-NH_2 nanofibers *via* an amide reaction. The UV-vis spectrum of Probe 1 shows a typical absorption peak around 260 nm (Figure S4). CaF_2:Yb,Ho@SiO_2-NH_2 nanofibers exhibited a 'plain' absorption spectrum, implying that the nanofibers unconjugated with Probe 1 merely absorb light from λ= 230 to 300 nm. However, in the case of the Probe 1-conjugated CaF_2:Yb,Ho@SiO_2-NH_2 nanofibers (CaF_2:Yb,Ho@SiO_2-Probe 1), successful conjugation was confirmed by a new broad peak in the UV-vis absorption spectrum at λ=265 nm, and this was further supported by the negative zeta potential of CaF_2:Yb,Ho@SiO_2-Probe 1 (– 8.6 mV) resulting from presence of the negatively charged oligonucleotide strand.

2.4 Conjugation of Probe 2 with AuNPs

The AuNPs were synthesized by a seed-mediated method.[45] As shown in Figure 5a, the synthesized AuNPs had an average diameter of 16.3±2.1 nm. The lattice d-spacing calculated from the HRTEM image is 0.235 nm, corresponding to the (111) crystal plane of gold (JCPDS No. 04-0784).

In our design, a thiol group-modified probe (Probe 2) was immobilized on the surface of the AuNPs *via* an Au-S bond. The zeta potential of the pure AuNPs was +20.8 mV due to the CTAB layer, but this reversed to -9.4 mV after the formation of the AuNP-Probe 2 conjugation (Figure 4b). This surface charge reversal appeared to confirm that functionalization achieved as intended. This result is further supported by UV-vis

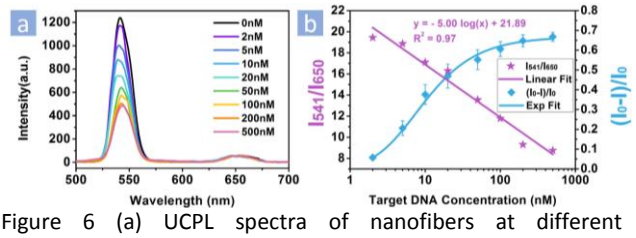

Figure 6 (a) UCPL spectra of nanofibers at different concentrations of target miRNA. (b) Linear relationship between the intensity ratio I_{541}/I_{650} and the concentration of target miRNA (purple); Exponential relationship between the quenching UCPL intensity at 541 nm and the concentration of target miRNA (blue).

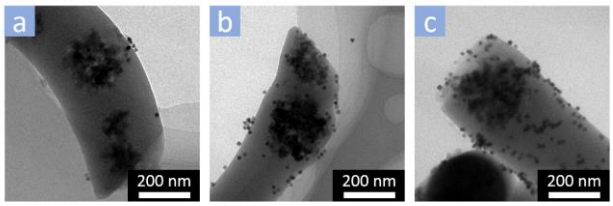

Figure 7 TEM images of AuNPs- Probe 2 conjugated with CaF_2:Yb,Ho@SiO_2upon different concentrations of target miRNA: (a) 0, (b) 50 nM, (c) 500 nM.

absorption measurements (Figure 5b). The absorption peak for the AuNPs was found to be located at ~535 nm and the small absorption peak at around 300 nm was due to the CTAB coating. After oligonucleotide conjugation, AuNP-Probe 2 spectrum showed clear evidence of absorbance at 260 nm, confirming the successful immobilization of Probe 2 on the AuNPs.

A key result is that the UV-vis absorption spectrum of AuNPs-Probe 2 overlaps exactly with the strong green emission of the CaF_2:Yb,Ho@SiO_2 nanofibers. This is essential for the FRET effect to occur.

2.5 Detection of miRNA

The conjugation results presented above, show that it is possible to achieve a FRET effect between the CaF_2:Yb,Ho@SiO_2 – Probe 1 (energy donor) and AuNP- Probe 2 (energy acceptor). In addition, the green emission is much stronger as compared with the red emission, which is ideal for application as an energy donor in FRET-based analysis. A membrane made of Probe 1-containing CaF_2:Yb,Ho@SiO_2 nanofibers and Probe 2-conjugated AuNPs was placed in a 20 mL glass bottle containing 2 mL de-ionised water. The target miRNA was then added and co-hybridization occurred between the target miRNA and the oligonucleotides. The nanofibers and AuNPs were consequently brought into close proximity, triggering the FRET effect. As shown in Figure 6a, the intensity of green emission at 541 nm was quenched significantly, whereas the red emission at 650 nm remained unchanged, indicating energy transfer from the green emission of photoluminescent nanofibers to AuNPs. The green emission intensity decreased by about 60 % when the concentration of target miRNA was 500 nM. This was due to strong absorption by the AuNP-Probe 2 combination at 541 nm and very low absorption at 650 nm. As the concentration of target miRNA was increased, the intensity of green emission decreased. Generally, FRET will occur when the distance between donors and acceptors is below 10 nm.[46-48] In this work, it is proposed that, with increasing miRNA concentration, increasing numbers of AuNPs were brought into close proximity and conjugated with the nanofibers to provide a suitable acceptor-to-donor distance for FRET to occur and this was characterized by quenching of the green emission (Figure 7).

To explore the quenching efficiency of the FRET system, different miRNA concentrations, ranging from 2 nM – 500 nM, were tested. Figure 6b shows the relationship between the quenching of

emission intensity ΔI ($\Delta I=(I_0-I)/I_0$) and the concentration of target miRNA (where I_0 and I represent the green emission intensity of CaF_2:Yb,Ho@SiO_2 nanofibers in the absence and presence of different concentrations of target miRNA, respectively). The quenching efficiency increased with increasing target miRNA concentration and the intensity ratio (I_{541}/I_{650}) was found to vary linearly with the concentration of target miRNA. At a miRNA concentration of 500 nM, the quenching efficiency reached a value of 67 %.

3 Conclusions

In summary, a novel UCPL-based FRET biosensor utilizing amino-modified CaF_2:Yb,Ho@SiO_2 nanofibers and AuNPs was developed for miRNA-195 detection. The sandwich structure formed as a result of co-hybridization of target miRNA *via* the action of oligonucleotides allowed the nanofibers and AuNPs to be brought into sufficiently close proximity to trigger a FRET effect. The intensity ratio of green to red emission, I_{541}/I_{650}, varied linearly with miRNA concentration, allowing the result to be utilized as a standard curve for quantitative determination target miRNA. This work demonstrates the feasibility of using co-conjugated probes, AuNPs and nanofibers that can be processed to form a membrane. Further work will investigate the use of multiple combinations of upconversion photoluminescent particle-impregnated nanofibers for the simultaneous detection of several biomarkers, relevant to early stage cancer diagnosis.

4 Materials and Methods

4.1 Synthesis of CaF_2:Yb,Ho Nanoparticles

CaF_2:Yb,Ho nanoparticles were prepared using a hydrothermal process based on a method reported by Deng *et al.* (2015).[49] Calcium nitrate tetrahydrate ($Ca(NO_3)_2{\cdot}4H_2O$, 1mmol, A.R., Sinopharm Chemical, China), ytterbium nitrate pentahydrate ($Yb(NO_3)_3{\cdot}5H_2O$, 0.2125 mmol, 99.9 %, Sigma-Aldrich), holmium nitrate pentahydrate ($Ho(NO_3)_3{\cdot}5H_2O$, 0.0375 mmol, 99.9 %, Sigma-Aldrich), trisodium citrate (Cit^{3-}, 2 mmol, 99.0 %, Aladdin) and sodium fluoroborate ($NaBF_4$, 2 mmol, 99.99 %, Aladdin) were dissolved in 40 mL of deionized water and ammonia solution was added to maintain the pH at 7.0. The solution was transferred into a 50 ml stainless-steel Teflon autoclave and maintained at 180 °C for 24 h. The precipitate obtained was collected by centrifugation, washed and dried at 80 °C for 24 h to obtain CaF_2:Yb,Ho nanoparticles. The CaF_2:Yb,Ho nanoparticles obtained were then calcined at 700 °C for 4 h.

4.2 Fabrication of CaF_2:Yb,Ho@SiO_2 Nanofibers

1.67 g of tetraethyl orthosilicate (TEOS, A.R., Sinopharm Chemical, China), 200 µL of acetic acid (A.R., Sinopharm Chemical, China), 600 µL of deionized water and 10 mL of ethanol (99.9 vol %, Sinopharm Chemical, China) were mixed by stirring for 1.5 h. Then 1.5 mL of N,N-dimethylformamide (DMF, A.R., Sinopharm Chemical, China), 1.2 g of polyvinylpyrrolidone (PVP, Mw =1 300 000, Aladdin), and 50 mg of the calcined CaF_2:Yb,Ho nanoparticles were added and stirred for 2 h to obtain the electrospinning precursor.

For the electrospinning process, the precursor solution was transferred into a single nozzle electrospinning setup. The flow rate was set at 1.5 mL/h. The distance and the high voltage between the needle tip and the collector were set at 15 cm and 8-11 kV, respectively. The as-spun composite nanofibers were dried at 80 °C overnight and calcined at 600 °C for 4 h.

4.3 Functionalization of CaF_2:Yb,Ho@SiO_2 Nanofibers with Amino Groups

100 mg of CaF_2:Yb,Ho@SiO_2 nanofibers and 0.8 mL of 3-aminopropyl-triethoxysilane (APTES, 99 %, Macklin) were dispersed in 40 mL of DMF and stirred at 80 °C for 24 h. Then the nanofibers were centrifuged and washed three times with DMF to obtain amino modified CaF_2:Yb,Ho@SiO_2 nanofibers (CaF_2:Yb,Ho@SiO_2-NH_2).

4.4 Conjugation of Probe 1 with CaF_2:Yb,Ho@SiO_2 Nanofibers

In order to covalently conjugate Probe 1 to CaF_2:Yb,Ho@SiO_2-NH_2 nanofibers, carboxyl group-modified miRNA-capturing oligonucleotide 1 (Probe 1, 5'-COOH AAAAAGCCAATATTTC-3', 25 µL, 100 µM, Sangon Biotechnology Co., Ltd. Shanghai, China), N-hydroxy-succinimide (NHS, 200 µL, 2 mg/mL, 97.0～102.0 %, Sinopharm Chemical, China) and 1-ethyl-3-(3-dimethylaminopropy) carbodiimide (EDC, 400 µL, 2 mg/mL, 98.0 %, Aladdin) were incubated in 2.5 mL of ultrapure water at 37 °C for 1 h. Then, 5 mg of CaF_2:Yb,Ho@SiO_2-NH_2 nanofibers were added into the solution and reacted at 37 °C for 24 h. The conjugates formed were centrifuged with water three times and then redispersed in 800 µL of water.

4.5 Synthesis of Gold Nanoparticles

4.5.1 Seed Solution

The gold nanoparticles (AuNPs) were fabricated according to a modified version of the well-established seed-mediated growth method.[45] Briefly, CTAB aqueous solution (5 mL, 0.2 M, A.R., Sinopharm Chemical, China) was mixed with $HAuCl_4$ (5 mL, 0.5 mM, A.R. Sinopharm Chemical, China) and ice-cold $NaBH_4$ (0.6 mL, 0.01 M, 96 %, Sinopharm Chemical, China) under vigorous stirring for 2 min. Then the brownish-yellow seed solution was aged at room temperature for 3 h before use.

4.5.2 Growth Solution

The growth solution was made from solutions of CTAB (0.2 M, 6 mL), $HAuCl_4$ (0.5 mM, 6 mL), and ascorbic acid (0.1 M, 4.5 mL, 99.7 %, Sinopharm Chemical, China). The gold seed solution (0.3 mL) was then injected into the growth solution and the mixture was stirred for 1 h and left undisturbed overnight. The AuNPs obtained were centrifuged to remove excess CTAB and ascorbic acid, re-suspended and concentrated 50-fold in 0.005 M CTAB solution for the following experiments.

4.6 Synthesis of AuNP-Probe 2 Conjugation

The modification of AuNPs was conducted following a modified version of protocols reported previously by Yi *et al*., Xu *et al*., Liu *et al*. and Zhang *et al.* [50-53] A volume of 60 µL, 100 mM thiol-modified miRNA-capturing oligonucleotide 2 (Probe 2, 5' TGTGCTGCTAAAAAA SH-3', Sangon Biotechnology Co., Ltd. Shanghai, China) was pipetted into a micro centrifuge tube. Then 1

µL of 10 mM fresh Tris-(2-carboxyethyl) phosphine hydrochloride (TCEP, ≥ 98 %, Sigma-Aldrich.) was added to the tube to activate the thiol-modified Probe 2. The sample was incubated at room temperature for 1 h, before 300 µL of the prepared AuNP solution into the tube. The mixture was then allowed to react at 25 °C for at least 16 h in the dark with gentle shaking. After incubation, the conjugate was collected after three consecutive purification cycles comprising centrifugation for 10 min at 6000 rpm and redispersed in 0.005 M CTAB buffer. The conjugate was stored at 4 °C.

4.7 Detection of Target MiRNA Based on the FRET System

800 µl of CaF_2:Yb,Ho@SiO_2-NH_2 –Probe 1 solution, 800 µl of AuNP-Probe 2, and 400 µL of target miRNA (miRNA 195, UAGCAGCACAGAAAUAUUGGC, Sangon Biotechnology Co., Ltd. Shanghai, China), with concentrations ranging from 2 nM to 500 nM, were mixed and incubated at 25 °C for 1 h. The mixture was centrifuged, washed twice with water and re-suspended in 2 mL of water.

4.8 Characterization

The morphologies and microstructures of the CaF_2:Yb,Ho nanoparticles, CaF_2:Yb,Ho@SiO_2 nanofibers, AuNPs, and AuNPs conjugated CaF_2:Yb,Ho@SiO_2 nanofibers were characterized using field emission scanning electron microscopy (FESEM, SU-70, Hitachi) and high-resolution transmission electron microscopy (HRTEM, Tecnai F20, FEI). The XRD patterns were recorded using a RIGAKU D/MAX 2550/PC multi crystal diffractometer. FTIR spectra were measured on a Perkin-Elmer 580B (Tensor 27, Bruker) infrared spectrophotometer using the KBr pellet technique. UV-vis spectroscopy measurements were performed on TU-1810 UV-vis spectrophotometer. Measurements of zeta potential were collected on a zetasizer (Zetasizer 3000 HSA, Malvern). Diluted aqueous solution of samples were performed in quintuplicates. The UCPL spectra were obtained under the excitation of a continuous laser with a wavelength of 980 nm from a fluorescence spectrophotometer (PL, FLSP920, Edinburgh). The diameter distributions were obtained by stochastically choosing and measuring of fifty fibers from SEM images.

Acknowledgements

This work was financially supported by the National Nature Science Foundation of China (51232006 and 51672247), the '111' Program funded by Education Ministry of China and State Administration of Foreign Experts Affairs (B16043), the Major State Research Program of China (2016YFC1101900), and the Nature Science Foundation of Zhejiang Province (LY15E020005).

Notes and references

1. L. A. Torre, F. Bray, R. L. Siegel, J. Ferlay, J. Lortet-Tieulent and A. Jemal, *CA-Cancer J. Clin.*, 2015, **65**, 87-108.
2. D. P. Bartel, *Cell*, 2004, **116**, 281-297.
3. N. Bushati and S. M. Cohen, *Annu. Rev. Cell Dev. Biol.*, 2007, **23**, 175-205.
4. W. Liu, S.-Y. Mao and W.-Y. Zhu, *World journal of gastroenterology*, 2007, **13**, 497.
5. R. Garzon, G. A. Calin and C. M. Croce, *Annu. Rev. Med.*, 2009, **60**, 167-179.
6. X. Chen, Y. Ba, L. Ma, X. Cai, Y. Yin, K. Wang, J. Guo, Y. Zhang, J. Chen, X. Guo, Q. Li, X. Li, W. Wang, Y. Zhang, J. Wang, X. Jiang, Y. Xiang, C. Xu, P. Zheng, J. Zhang, R. Li, H. Zhang, X. Shang, T. Gong, G. Ning, J. Wang, K. Zen, J. Zhang and C.-Y. Zhang, *Cell Res.*, 2008, **18**, 997-1006.
7. J. Li, S. Tan, R. Kooger, C. Zhang and Y. Zhang, *Chem. Soc. Rev.*, 2014, **43**, 506-517.
8. L. Liu, L. Chen, Y. Xu, R. Li and X. Du, *Biochem. Biophys. Res. Commun.*, 2010, **400**, 236-240.
9. H. M. Heneghan, N. Miller, A. J. Lowery, K. J. Sweeney, J. Newell and M. J. Kerin, *Annals of Surgery*, 2010, **251**, 499-505.
10. H. M. Heneghan, N. Miller, R. Kelly, J. Newell and M. J. Kerin, *The Oncologist*, 2010, **15**, 673-682.
11. P. S. Mitchell, R. K. Parkin, E. M. Kroh, B. R. Fritz, S. K. Wyman, E. L. Pogosova-Agadjanyan, A. Peterson, J. Noteboom, K. C. O'Briant, A. Allen, D. W. Lin, N. Urban, C. W. Drescher, B. S. Knudsen, D. L. Stirewalt, R. Gentleman, R. L. Vessella, P. S. Nelson, D. B. Martin and M. Tewari, *Proceedings of the National Academy of Sciences*, 2008, **105**, 10513-10518.
12. K. E. Resnick, H. Alder, J. P. Hagan, D. L. Richardson, C. M. Croce and D. E. Cohn, *Gynecologic Oncology*, 2009, **112**, 55-59.
13. M. Lin, P. Song, G. Zhou, X. Zuo, A. Aldalbahi, X. Lou, J. Shi and C. Fan, *Nat. Protocols*, 2016, **11**, 1244-1263.
14. S. Husale, H. H. J. Persson and O. Sahin, *Nature*, 2009, **462**, 1075-1078.
15. Q. Wang, R. Liu, X. Yang, K. Wang, J. Zhu, L. He and Q. Li, *Sensors Actuators B: Chem.*, 2016, **223**, 613-620.
16. Z. Jin, D. Geißler, X. Qiu, K. D. Wegner and N. Hildebrandt, *Angew. Chem. Int. Ed.*, 2015, **54**, 10024-10029.
17. Y. Liu, M. Wei, Y. Li, A. Liu, W. Wei, Y. Zhang and S. Liu, *Anal. Chem.*, 2017, **89**, 3430-3436.
18. Q. Wang, B.-C. Yin and B.-C. Ye, *Biosens. Bioelectron.*, 2016, **80**, 366-372.
19. J. Shi, C. Chan, Y. Pang, W. Ye, F. Tian, J. Lyu, Y. Zhang and M. Yang, *Biosens. Bioelectron.*, 2015, **67**, 595-600.
20. L. Wang, J. Liu, Y. Dai, Q. Yang, Y. Zhang, P. Yang, Z. Cheng, H. Lian, C. Li, Z. Hou, P. a. Ma and J. Lin, *Langmuir*, 2014, **30**, 13042-13051.
21. Y. Li, Y. Zhou, T. Gu, G. Wang, Z. Ren, W. Weng, X. Li, G. Han and C. Mao, *Particle & Particle Systems Characterization*, 2016, **33**, 896-905.
22. Y. Fu, X. Li, C. Sun, Z. Ren, W. Weng, C. Mao and G. Han, *ACS Appl. Mater. Interfaces*, 2015, **7**, 25514-25521.
23. H. Liu, Y. Fu, Y. Li, Z. Ren, X. Li, G. Han and C. Mao, *Langmuir*, 2016, **32**, 9083-9090.
24. Y. Fu, C. Fang, Z. Ren, G. Xu, X. Li and G. Han, *Chem-Eur J*, 2017, **23**, 2423-2431.
25. H. J. M. A. A. Zijlmans, J. Bonnet, J. Burton, K. Kardos, T. Vail, R. S. Niedbala and H. J. Tanke, *Anal. Biochem.*, 1999, **267**, 30-36.
26. S. Wu, G. Han, D. J. Milliron, S. Aloni, V. Altoe, D. V. Talapin, B. E. Cohen and P. J. Schuck, *Proc. Natl. Acad. Sci. U.S.A.*, 2009, **106**, 10917-10921.
27. H. Du, J. Yu, D. Guo, W. Yang, J. Wang and B. Zhang, *Langmuir*, 2016, **32**, 1155-1165.
28. B. Liu, C. Li, B. Xing, P. Yang and J. Lin, *J. Mater. Chem. B*, 2016, **4**, 4884-4894.

29. Q. Han, Z. Dong, X. Tang, L. Wang, Z. Ju and W. Liu, *J. Mater. Chem. B*, 2017, **5**, 167-172.
30. Y. Dai, H. Bi, X. Deng, C. Li, F. He, P. a. Ma, P. Yang and J. Lin, *J. Mater. Chem. B*, 2017, **5**, 2086-2095.
31. Y. Li, Y. Zhou, X. Li, J. Sun, Z. Ren, W. Wen, X. Yang and G. Han, *RSC Advances*, 2016, **6**, 38365-38370.
32. N.-N. Dong, M. Pedroni, F. Piccinelli, G. Conti, A. Sbarbati, J. E. Ramírez-Hernández, L. M. Maestro, M. C. Iglesias-de la Cruz, F. Sanz-Rodriguez, A. Juarranz, F. Chen, F. Vetrone, J. A. Capobianco, J. G. Solé, M. Bettinelli, D. Jaque and A. Speghini, *ACS Nano*, 2011, **5**, 8665-8671.
33. B. Zhou, L. Tao, Y. H. Tsang and W. Jin, *J. Mater. Chem. C*, 2013, **1**, 4313-4318.
34. W. Zheng, S. Zhou, Z. Chen, P. Hu, Y. Liu, D. Tu, H. Zhu, R. Li, M. Huang and X. Chen, *Angew. Chem.*, 2013, **125**, 6803-6808.
35. F. Perche, Y. Yi, L. Hespel, P. Mi, A. Dirisala, H. Cabral, K. Miyata and K. Kataoka, *Biomaterials*, 2016, **90**, 62-71.
36. W. Hou, P. Wei, L. Kong, R. Guo, S. Wang and X. Shi, *J. Mater. Chem. B*, 2016, **4**, 2933-2943.
37. K. A. Fitzgerald, K. Rahme, J. Guo, J. D. Holmes and C. M. O'Driscoll, *J. Mater. Chem. B*, 2016, **4**, 2242-2252.
38. M. Wang, W. Hou, C.-C. Mi, W.-X. Wang, Z.-R. Xu, H.-H. Teng, C.-B. Mao and S.-K. Xu, *Anal. Chem.*, 2009, **81**, 8783-8789.
39. J. G. Jesu Raj, M. Quintanilla, K. A. Mahmoud, A. Ng, F. Vetrone and M. Zourob, *ACS Appl. Mater. Interfaces*, 2015, **7**, 18257-18265.
40. S. Wu, N. Duan, X. Li, G. Tan, X. Ma, Y. Xia, Z. Wang and H. Wang, *Talanta*, 2013, **116**, 611-618.
41. Z. Xia, Y. Fu, T. Gu, Y. Li, H. Liu, Z. Ren, X. Li and G. Han, *Materials & Design*, 2017, **119**, 85-92.
42. F. He, P. Yang, D. Wang, C. Li, N. Niu, S. Gai and M. Zhang, *Langmuir*, 2011, **27**, 5616-5623.
43. C. Ma, X. Xu, F. Wang, Z. Zhou, D. Liu, J. Zhao, M. Guan, C. I. Lang and D. Jin, *Nano Lett.*, 2017, **17**, 2858-2864.
44. B. Zhou, B. Shi, D. Jin and X. Liu, *Nat Nano*, 2015, **10**, 924-936.
45. R. Contreras-Cáceres, A. Sánchez-Iglesias, M. Karg, I. Pastoriza-Santos, J. Pérez-Juste, J. Pacifico, T. Hellweg, A. Fernández-Barbero and L. M. Liz-Marzán, *Adv. Mater.*, 2008, **20**, 1666-1670.
46. Q. Su, W. Feng, D. Yang and F. Li, *Acc. Chem. Res.*, 2016.
47. V. Muhr, C. Würth, M. Kraft, M. Buchner, A. J. Baeumner, U. Resch-Genger and T. Hirsch, *Anal. Chem.*, 2017, **89**, 4868-4874.
48. Y. Fu, X. Chen, X. Mou, Z. Ren, X. Li and G. Han, *ACS Biomater.-Sci. Eng.*, 2016, **2**, 652-661.
49. X. Deng, Y. Dai, J. Liu, Y. Zhou, P. a. Ma, Z. Cheng, Y. Chen, K. Deng, X. Li, Z. Hou, C. Li and J. Lin, *Biomaterials*, 2015, **50**, 154-163.
50. Y. Yi, H. Wang, X. Wang, Q. Liu, M. Ye and W. Tan, *ACS Appl. Mater. Interfaces*, 2017, **9**, 5847-5854.
51. L. Xu, H. Kuang, C. Xu, W. Ma, L. Wang and N. A. Kotov, *J. Am. Chem. Soc.*, 2012, **134**, 1699-1709.
52. J. Liu and Y. Lu, *Nat. Protocols*, 2006, **1**, 246-252.
53. J. Zhang, S. Song, L. Wang, D. Pan and C. Fan, *Nat. Protocols*, 2007, **2**, 2888-2895.